IJAF - Instrumentcenter for Jordbaseret Astronomisk Forskning
Astronomisk Observatorium, Juliane Maries Vej 30, DK-2100 København Ø, Danmark.

Astronomical Instrument Centre

IJAF technical report #7:

2nd edition for the 2nd commissioning run

Characterization of the Mosaic Camera

4k by 4k CCD array

by

Anton Norup Sørensen

October, 2002

Contents

1 Introduction

This report presents the results from characterization of the mosaic CCD camera (MOSCA) built by Copenhagen University Observatory / IJAF for the Nordic Optical Telescope.

The mosaic is a two by two arrangement of Loral/Lesser 2048 by 2048 pixel CCDs. The total imaging array is then 4096 by 4096 pixels, each pixel is 15μm square.

The controller contains a two-channel video board and a clock generator for each CCD. The sequence of boards and cables should not be changed as each is optimized for the individual CCD.

The characterization was in part done on the individual detectors and in part on the assembled array. Results from individual tests are only included where they are certain to be in agreement with an array test.

During the first commissioning run in January 2002, an electrical failure occurred. An output on one of the CCDs was damaged, and during repairs in Copenhagen another CCD was completely destroyed. As no spare CCDs with two working outputs are available, the mosaic is now primarily to be used with only one output per CCD.

This report replaces the original commissioning report, but contains much data from it. Here, the performance of the three original quadrants is verified and the characteristics of the replaced CCD is described.

2 Array flatness

In order to provide a sharp image, the detector must conform to the focal plane. The curvature of the focal plane is corrected by a field flattener window for direct imaging. The focal reducer (FRED) corrects focal plane curvature by itself, so a flat mosaic window has to be used in this case. The remaining task is to align the CCD array with the flattened focal plane.

The individual CCDs are not quite equal in thickness and may also be slightly tilted and warped. This is mostly due to the glueing of the thinned photo-sensitive layer onto the substrate, that is again glued onto an Invar base.

The four CCDs were each mounted on another Invar base and then mounted on a common steel plate, machined as flat as possible. The array was then taken to ESO, Garching, and the height of the surface was mapped using their mosaic measuring machine, with the kind help from its designer, Stefan Ströbele. The shape of the steel plate was also measured using the ESO machine, and the measurement was repeated using an in-house mechanical device. The steel plate was replaced by a final mounting plate made of Invar. This was measured mechanically, and now a map could be calculated of the mosaic detector surface, taking into account the differences between the steel and Invar plates. The peak-to-peak deviation from flatness was found to be $95\mu m$.

The four bases between the CCDs and the mounting plate could now be machined to compensate for the measured deviations from flatness. When machining was complete, the deviations of the base thicknesses from the target values were $10\mu m$ RMS.

After the first commissioning run, the CCD 9-(0,1) was replaced with W20-(0,0). The array height was mapped two more times in Garching, this time with the help from Sebastian Deiries and Fabrice Christen. After the second measurement, deviations were found small enough to require no more machining of the base plates. The result of the final measurement is shown in figures 1 and 2. This map indicates a P-P deviation from co-planarity of $25\mu m$ using a plane fit to each quadrant, increasing to $35\mu m$ when including warping of the CCDs.

The last task is to align the detector plane with the focal plane. The overall tilt of the mounting plate relative to the camera mounting flange was measured by examining the reflection angle of light incident on the window and on the CCDs. The tilt of the mounting plate was then adjusted until the

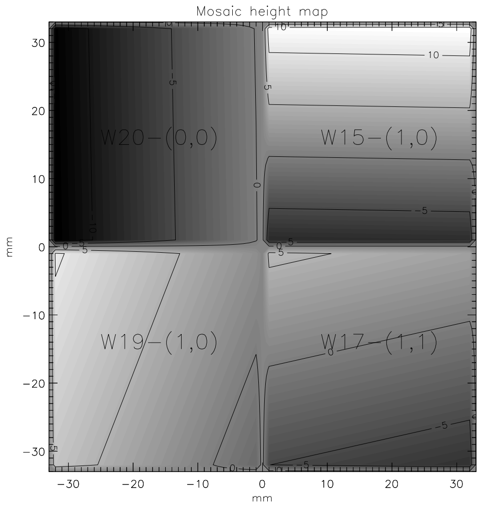

Figure 1: Map showing the deviation from co-planarity of the array, with peak-to-peak amplitude of $25\mu m$. Each quadrant is represented by a flat surface. Note that the orientation shown here differs from that used in the rest of the report.

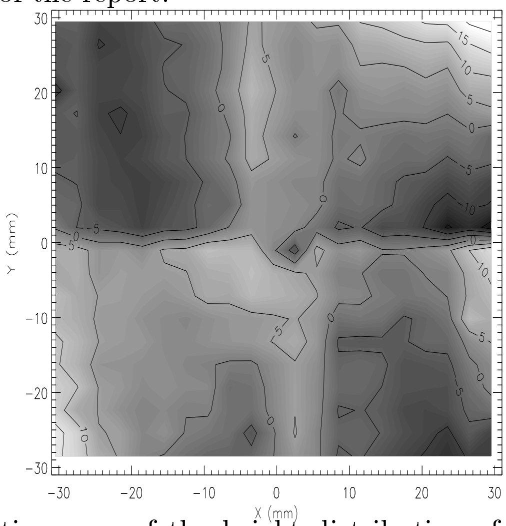

Figure 2: A higher resolution map of the height distribution of the detector surfaces. An average tilt have been subtracted and interpolated points are replacing the measurements affected by the gap between the detectors. The peak-to-peak amplitude is $35\mu m$. Orientation is as in the figure above.

two reflected beams almost coincided. In this way, the global tilt of the array was reduced to below 1', or no more than $18\mu m$ P-P for the 6.2cm side length.

All measurements were made at room temperature. Some deformation could occur when cooling the array to its operating temperature of -100°C.

The edges of the four detectors are placed approximately half a millimetre from each other. The distance is somewhat irregular, as no precise control could be made during the replacement of the damaged CCDs. During this process, all available slack in the mounting holes was used to increase the distance between the CCDs.

3 Operating options

While each CCD is born with two amplifiers, two of the installed detectors only have one functional amplifier. This still leaves a lot of possible read-out configurations. 13 configurations that allows complete read-out of the field a supported, and a further 8 are available, where only partial read-out is possible due to the damaged outputs.

In figure 3 the array is shown in the orientation also used in the BIAS/SAOimage display. The four detectors are labeled according to their wafer numbers, but for a more intuitive use during read-out configuration, the four quadrants are named after compass directions, with north at the top and east to the right. The two amplifiers are labeled "L" and "R" according to whether they are located on the left or right side of the CCD. Each amplifier is also labeled by a number from 0 to 7. These numbers are used when the bias level is set by sending direct commands to the controller.

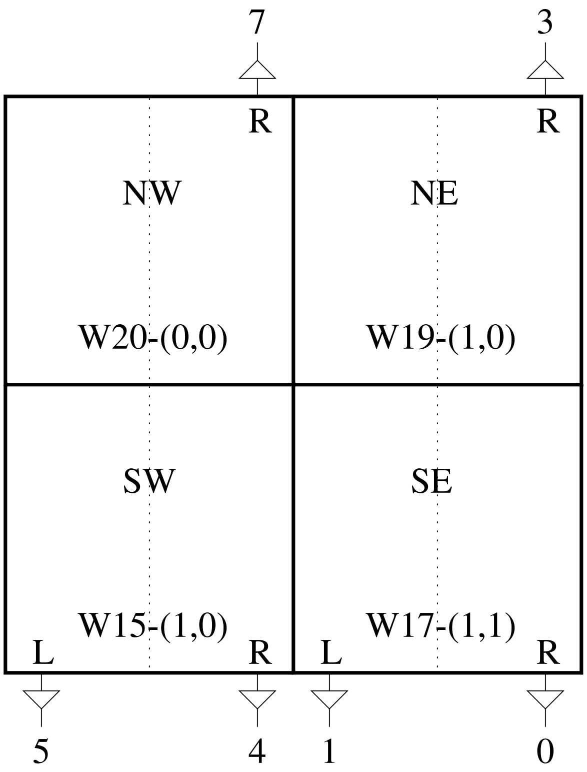

Figure 3: Nomenclature for the CCD and amplifier layout. Compass directions and L/R are used for read-out configuration. Amplifier numbers are used when setting the bias level.

The available read-out modes are listed below. Modes written in italics will be affected by the damaged outputs.

Name	Alias	# CCDs	# outputs	Location	
A48	*A28*	4	8	*All*	
A4RL	*A24*	4	4	*South: Right*	*North: Left*
A4LR	A25	4	4	South: Left	North: Right
A4RR	A26	4	4	South: Right	North: Right
A4LL	*A27*	4	4	*South: Left*	*North: Left*
A2SR	A20	2	2	South-West: Right	South-East: Right
A2SL	A21	2	2	South-West: Left	South-East: Left
A2NL	*A22*	2	2	*North-West: Left*	*North-East: Left*
A2NR	A23	2	2	North-West: Right	North-East: Right
A1NWR	A30	1	1	North-West: Right	
A1NWL	*A31*	1	1	*North-West: Left*	
A1NW2	*A32*	1	2	*North-West: Both*	
A1NER	A33	1	1	North-East: Right	
A1NEL	*A34*	1	1	*North-East: Left*	
A1NE2	*A35*	1	2	*North-East: Both*	
A1SWR	A36	1	1	South-West: Right	
A1SWL	A37	1	1	South-West: Left	
A1SW2	A38	1	2	South-West: Both	
A1SER	A39	1	1	South-East: Right	
A1SEL	A40	1	1	South-East: Left	
A1SE2	A41	1	2	South-East: Both	

Of these, the recommended mode for reading out the entire array is "A4RR" due to the better bias level stability in the southern half.

Read-out time is 108 sec when using one output per quadrant, and 54 sec when using two.

It is recommended to always use MPP mode.

High gain should be used for 1x1 binning, and low gain for 2x2 and stronger binning.

If desired, it is possible to move the flat window of FREC to MOSCA by swapping the flanges. Due to an asymmetry in the position of the eight screws holding the flange onto the camera house, a circular mark on the front of the FREC flange has to be aligned with the temperature sensor plug on MOSCA.

4 Cosmetics

Combining the field of four CCD detectors to act as a single unit increases the demands to response uniformity of the detectors. A thinned Loral CCD typically has degraded sensitivity and uniformity near the edges, influencing perhaps 10% of the total area. In a mosaic, these edges now also occupy the central area of the total field. When selecting the position and orientation of the CCDs, care was taken to place the least uniform edges at the edges of the combined field. Due to the location of the read-out amplifiers, bad columns unfortunately will have to predominantly occupy the central region of the field.

Flat fields for wavelengths of 1060nm, 550nm and 334nm are shown in figures 4, 5 and 6, respectively.

The average level is a little different in each quadrant. This is in part due to variations in the gain from each amplifier, although these have been adjusted to be close to each other. Another reason is differences in overall quantum efficiency. E.g., the SW quadrant appears to have higher sensitivity at

334nm than the others.

In the 550nm image, the overall structure is flat to within ±1%. Spread over the array are small spots where the sensitivity can drop by 10%, and sometimes more. These spots are more frequent near the edges of the CCDs. Specks of dust on the window appear as circular disks or "worms".

At 334nm, the flat field structure is similar to the 550nm flat. Over the majority of the area, deviation from flatness is still within ±1%, but the irregularities seen at 550nm are now stronger, and a few new ones are appearing.

At 1060nm, almost at the near-IR cut-off, the response becomes increasingly inhomogeneous. The typical variation is ±3%, increasing to 10% at the edges. This is primarily due to spatial variations in the reflection of the support structure below the detecting layer.

Charge traps and bad columns can be found by comparing a flat field exposure at very low illumination level to a well exposed one, as illustrated in figure 7. Several exposures at 50e- and 50Ke- were combined to produce two high S/N flat field maps for the comparison. Several bad columns can be identified both in the high level flat and in this ratio image. The ratio also shows traps as short vertical lines and a few areas where proper flat fielding failed due to very low sensitivity.

Below is a table of the number of bad columns and traps found. This only gives a crude impression of the cosmetic quality, as the severity of the defects varies.

CCD	Corner	Bad columns	Traps
W15-(1,0)	**SW**	≈ 30	6
W17-(1,1)	**SE**	≈ 50	11
W19-(1,0)	**NE**	15	7
W20-(0,0)	**NW**	23	11

5 Gain, linearity and full-well

Gain, the conversion factor between Analog to digital units (ADU) and electrons was determined from photon noise statistics. The graphs for this analysis are shown in figures 8 and 9, where gain at various levels of illumination is plotted.

The following conversion factors were found from the average values of the graphs:

	CCD	Corner	Left amplifier	Right amplifier
	W15-(1,0)	**SW**	1.27 e^-/ADU	1.27 e^-/ADU
High gain:	**W17-(1,1)**	**SE**	1.28 e^-/ADU	1.30 e^-/ADU
	W19-(1,0)	**NE**	N/A	1.30 e^-/ADU
	W20-(0,0)	**NW**	N/A	1.30 e^-/ADU

	CCD	Corner	Left amplifier	Right amplifier
	W15-(1,0)	**SW**	5.8 e^-/ADU	5.8 e^-/ADU
Low gain:	**W17-(1,1)**	**SE**	5.8 e^-/ADU	5.9 e^-/ADU
	W19-(1,0)	**NE**	N/A	5.9 e^-/ADU
	W20-(0,0)	**NW**	N/A	5.9 e^-/ADU

The almost identical gain values for each of the modes are the result of adjusting the gain to give a raw output image of good uniformity.

The high gain of 1.30 e^-/ADU is suitable for most observations, allowing the noise floor to be sampled well and covers most of the dynamic range up to saturation. The low gain value of about 6 e^-/ADU makes this mode suitable for 2x2 binning, where again the digital full well will be close to the blooming threshold.

Full well of each detector output has been determined from photon shot noise analysis, i.e. the full well is where the shot noise is seen to drop due to blooming. As some of the channels initially had a rather small full well, the voltages of each detector were optimized for the best full well in MPP mode.

CCD	Corner	Left amplifier	Right amplifier
W15-(1,0)	**SW**	$108Ke^-$	$106Ke^-$
W17-(1,1)	**SE**	$96Ke^-$	$112Ke^-$
W19-(1,0)	**NE**	N/A	$102Ke^-$
W20-(0,0)	**NW**	N/A	$\geq 52Ke^-$

The values given here are lower limits - in some cases full well may occur a few Ke^- higher. The same full well is found with MPP disabled.

For the W20-(0,0) detector, the full well depends strongly on the position on the array. E.g. in the central field used for the tests above, the full well is approximately $85Ke^-$, but degrades near the corners furthest away from the serial register, unfortunately worst near the centre of the mosaic field of view. To illustrate this, the central region of a flat field is shown in figure 12. At a level of $65Ke^-$, blooming full well is revealed as a vertical smear of the pixel structure in the corner of the NW quadrant which is W20-(0,0). This means that for exposure levels above about 40KADU/$52Ke^-$, one has to examine this quadrant carefully to ensure that full well has not been reached.

The improved full well was obtained by lowering the voltage of parallel phase no. 3 high state from the standard +4.0V to:

CCD	P3H
W15-(1,0)	+3.000V
W17-(1,1)	+2.625V
W19-(1,0)	+2.500V
W20-(0,0)	+2.300V

In addition, the low state of the parallel phases of W20-(0,0) were raised to -7.0V.

Gain determination from noise analysis is rarely precise enough for linearity measurements. Instead, linearity deviations are examined by measuring the ADU level versus exposure time, using a stable light source. Measurements made in this way are plotted in figures 10 and 11. By dividing the counts with the exposure time, corrected for shutter delay, a linear response should result in a constant level. Linearity was mapped from approximately $100e^-$ to full well, and shows the output to be linear within $\pm 0.15\%$ for all eight channels. The high gain data are noisier than the low gain data, but this is caused by the linearity measurement setup not being quite stable. From the high gain graphs, channel SER seems to perform comparatively poorly, but this appears to be due to bad columns in the region used for statistics, and not a general problem with this output.

6 Quantum-efficiency

The sensitivity has been measured through 11 narrow-band filters from 334nm to 1060nm and is plotted in figure 13 for each CCD. The data were extracted from an area of 400 by 400 pixels near the center of the detectors.

At long wavelengths where the detector is partially transparent, internal reflections will create fringes, making QE change rapidly with wavelength and making the local variations strong in monochromatic light. The effect sets in at about 650nm. At 830nm, the fringe amplitude is 15%. An example is shown in figure 14.

Stability of the sensitivity:

All four detectors have Mike Lesser's "Cat-C" Ag flash gate coating applied, with 550Å HfO_2 on top for protection and anti-reflection. This coating does not require any treatment to achieve high QE after warm-up.

During the time where the mosaic has been assembled in the laboratory, some variation in the QE has been noticed on all four detectors in the spots with very low sensitivity. In the large areas with high QE, the sensitivity remains stable. The variations are looked into below:

The detectors were first evaluated during the summer of 1998. The data from that time allow examination of the stability over a quite long period of four years. During most of this period, the detectors have been stored at room temperature, exposed to atmospheric air.

A degrading QE is unlikely to appear at a uniform rate over the detector. The most efficient method for checking QE stability is therefore to examine the ratio of flat fields obtained some time apart. The ratio of the old and present day flat fields at 334nm are shown in figure 15. The old flat fields were recorded in single-chip cameras, which is the cause for some difference in the distribution of scattered light. This creates a faint radial symmetric variation for each quadrant. Ignoring that, and shadows from moving dust, the global stability of the flat field is very good to less than one percent. There are however some strong local variations. What appears as clusters of white spots in the ratio image, is where the depth of low-sensitivity spots has decreased, improving the flat field uniformity. Especially on the western quadrants, many spots have weakened or even disappeared. Unfortunately, the QE has degraded in some of the larger, irregular low sensitivity spots. In a similar study performed in January 2002, a region of low sensitivity was present on the eastern edge of the SE quadrant. This has vanished since then. At longer wavelengths, the change in flat field structure is similar, although less pronounced.

7 Read-out noise

The following table shows the read-out noise (RON) found in different amplifier configurations for each detector.

W-15(1,0) / SW	Left amplifier	Right amplifier
High gain:	8.0 e^-	8.2 e^-
Low gain:	10.4 e^-	10.3 e^-

W-17(1,1) / SE	Left amplifier	Right amplifier
High gain:	8.8 e^-	8.2 e^-
Low gain:	11.2 e^-	10.5 e^-

W-19(1,0) NE	Left amplifier	Right amplifier
High gain:	N/A	8.0 e^-
Low gain:	N/A	10.7 e^-

W20-(0,0) / NW	Left amplifier	Right amplifier
High gain:	N/A	8.5 e^-
Low gain:	N/A	10.7 e^-

The average value of RON is 8.4e^- for high gain, and higher in low gain due to increased digitization noise. A typical high gain RON of 7.7e^- was at one time achieved in the laboratory, indication that a noise reduction from the present should be possible. The output of the NW detector shows some pick-up noise, and the left SE output has some faint horizontal lines appearing at random. The effect of this can be seen in the table, as these outputs have the highest noise.

8 Charge Transfer Efficiency

The fraction of electrons that are successfully moved from one pixel to another during read-out is described by the charge transfer efficiency (CTE).

The CTE has been measured using a ^{55}Fe X-ray source, whose emissions generate a specific number of photo-electrons on the CCD for each detection. The read-out counts as a function of position on the CCD can then be converted to a CTE value. Measurements were made at a detector temperature of -100°C.

The values found for the two read-out directions are:

W15-(1,0) / SW	Left amplifier	Right amplifier
Serial CTE:	1.000000	1.000000
Parallel CTE:	0.999997	0.999996

W17-(1,1) / SE	Left amplifier	Right amplifier
Serial CTE:	0.999998	1.000000
Parallel CTE:	0.999993	0.999992

W19-(1,0) / NE	Left amplifier	Right amplifier
Serial CTE:	N/A	1.000000
Parallel CTE:	N/A	0.999995

W20-(0,0) / NW	Left amplifier	Right amplifier
Serial CTE:	N/A	0.999998
Parallel CTE:	N/A	0.999995

In general, the CTE is very good. Within a measurement uncertainty of about $2 \cdot 10^{-6}$, the serial CTE is appears perfect. The parallel CTE is generally not quite so good, but still acceptable.

Note that CTE strictly speaking is a function of exposure level, so the value given here may not be applicable to all cases. Near zero level and full well, CTE may be poorer than the value given here.

9 Dark current

In order to minimize dark current, the detector should be operated at a temperature of -100°C. In addition, the detector design allows for Multi-Pinned-Phase operation, which further reduces the dark current. By default, the voltages are set for MPP mode.

The dark current listed below was determined from six half-hour exposures. There is no significant detection in MPP mode within the precision achievable from bias level subtraction. Overscan correction was not applied, increasing the uncertainty. Switching off MPP, an average dark current of $5e^-/h$ is recorded.

CCD	Corner	MPP	non-MPP	
W15-(1,0)	**SW**	-1	5	$e^-/h \pm 2e^-/h$
W17-(1,1)	**SE**	-1	6	$e^-/h \pm 2e^-/h$
W19-(1,0)	**NE**	1	1	$e^-/h \pm 2e^-/h$
W20-(0,0)	**NW**	2	5	$e^-/h \pm 2e^-/h$

A dark exposure is shown in figure 16. There are a few pixels and columns with high dark current. Most notable is a cluster of hot pixels in the lower right corner of the SW quadrant. These have a strength of up to 10 Ke^{-}/h in non-MPP mode, and typically less than half in MPP mode. Outside this area, other approx. 50 hot pixels can be found on the detector.

In the middle of the upper edge of the NW quadrant, a fan of light is seen. This is associated with a defect in the detector, and the brightness is depending on the voltage on the serial phases. The voltages have been adjusted to reduce the brightness of the defect while keeping the serial transfer good. The brightest part is about $1e^{-}$/minute/pixel and is rapidly falling off with distance. This quadrant is also seen to be affected by pick-up noise.

In the NE quadrant a hot pixel is saturating, and the charge starts blooming, filling column no. 1254. The saturation causes an offset in the bias level of the trailing pixels. The offset is less than 1 ADU, and falls off gradually. The area affected should be about proportional to the exposure time, as the blooming takes place during the exposure.

Also in the NE quadrant, a horizontal band pattern is seen, revealing a not quite stable bias level. The pattern can be expected to change randomly, probably requiring a more elaborate bias subtraction routine than what was applied here.

The malfunctioning amplifier in the left side of the NE quadrant is emitting light at normal operation voltages. Voltages have been reduced to a minimum, and the emission is now barely visible, partly hidden by the bias level fluctuations.

No change in the dark current structure was noted when switching to non-MPP mode.

10 Bias levels

Each output channel has its own bias level. This level may drift slightly due to circumstances like changing ambient temperature. While each read-out register is extended by two pixels, there are rarely reliable enough for a good bias level determination in a science exposure. It is recommended that extra overscan columns are added by the "xover" command if high precision bias level subtraction is required. Note that due to the limited amount of memory of the read-out buffer, adding overscan area will require removal of the same amount of imaging pixels.

There appears to be an intermittent problem with the bias levels - sometimes they are very flat, but at other times certain channels develop a large horizontal gradient. The problem affects especially the NE quadrant / output 3, that may show a gradient in excess of 200 ADU. This is illustrated in figure 17. Also shown is some level drift during the test sequence, showing the importance of using overscan reference. Read-out in A4RR mode is recommended, as the bias level appears more stable in the southern half than in A4LR mode. Minute fluctuations in the bias structure can be seen in the low-level flat field in figure 7.

It is convenient that the bias levels are close to each other to allow easy examination of the raw images. The bias level changes with the selection of different amplifier combinations, binning modes and MPP on/off. To allow easy switching between the modes, a script containing the appropriate bias level offsets should be made for each configuration expected to be used.

The bias level is set in the BIAS command prompt by entering commands of the form: "@BLm-maa+nnnnn", where "mm" is "HI" or "LO" for high- and low gain, respectively. "aa" is the amplifier number, as given in figure 3. "nnnnn" is a value to offset the bias level by. The conversion factor between the offset value and bias level in ADUs is -6.1. The target bias level for low gain should be about 50 ADU, as levels in some channels cannot go much higher than this. For high gain, a level of e.g. 300 ADU would be appropriate.

Some examples of common bias level scripts are given below, as a starting point. These will require some fine-tuning, depending on conditions.

1x1 binning, amplifier A4RR, mpp+, high gain
@BLHI00+02087
@BLHI03+01564
@BLHI04+01926
@BLHI07+01206

1x1 binning, amplifier ARR, mpp+, low gain
@BLLO00+00188
@BLLO03+00476
@BLLO04+00150
@BLLO07+00002

11 MTF

The Loral 2k3eb detectors have during their previous usage shown a problem with charge diffusion, resulting in degraded spatial resolution. As all measurements have given practically identical MTF results, no measurements were made on the particular detectors for the mosaic.

Instead, representative results from typical Loral 2k3eb detectors are presented. Data for measurement of the Modulation Transfer Function have been collected by measuring the contrast of interference fringes of different spatial frequency projected onto the CCD. The results are shown in figure 18. Three coincident sets are shown for 670nm illumination, and two sets for 830nm. As the absorption depth increases with longer wavelengths, the 830nm photo-electrons on average has to travel through a smaller part of the diffusion region, and thereby MTF is increased.

12 Cross-talk

As the read-out channels cannot be perfectly isolated from each other, cross-talk in the signal may occur. This was tested by imaging a bright point source on a section of the array assigned to one amplifier, and looking for an electronic "ghost image" in the signal from the other amplifiers. Ten images were summed to increase the sensitivity, and the spot then moved to examine another part of the array.

It was found that cross-talk is significant between the two amplifiers on each CCD, typically on a level of 10^{-4}. Cross-talk between CCDs is not seen, with an upper limit to the strength of 10^{-5}.

13 Camera house

The camera cryostat contains a 2.4 liter liquid Nitrogen tank, cooling the detector baseplate through a pair of copper braids. For the longest LN_2 holding time, a filler tube extension must be installed, and the camera must be looking at zenith during filling and kept vertical as long as practical afterwards. In vertical orientation, the LN_2 holding time is 48 hours at an ambient temperature of +23°C. Oriented horizontally, the holding time decreases to 22 hours. It is recommended that the tank is re-filled every day during operation, preferably in the morning.

The valve and pressure sensor are located close to the filling tube. Take care that LN_2 does not spill onto the fittings, as this may cause a vacuum leak or even crack the plastic fitting of the pressure sensor.

The two cold braids between the LN_2 tank and the detector baseplate have been cut as thin as possible in order to minimize LN_2 consumption. This means that the cool-down time from room temperature to -100°C is relatively long, about 8 hours.

An activated charcoal getter is attached to the LN_2 tank, cryo-pumping the dewar.

Pressure is measured using a Balzers sensor. The sensor is electrically insulated from the camera, and can be left on without creating interference noise.

In long dark exposures in the laboratory basement, the hit rate from energetic particles, "cosmics", was found to be 76 hits/cm^2/hour. From our statistical material, this appears to be a normal rate, i.e. there is no significant contribution to the hit rate from radioactive materials in the cryostat.

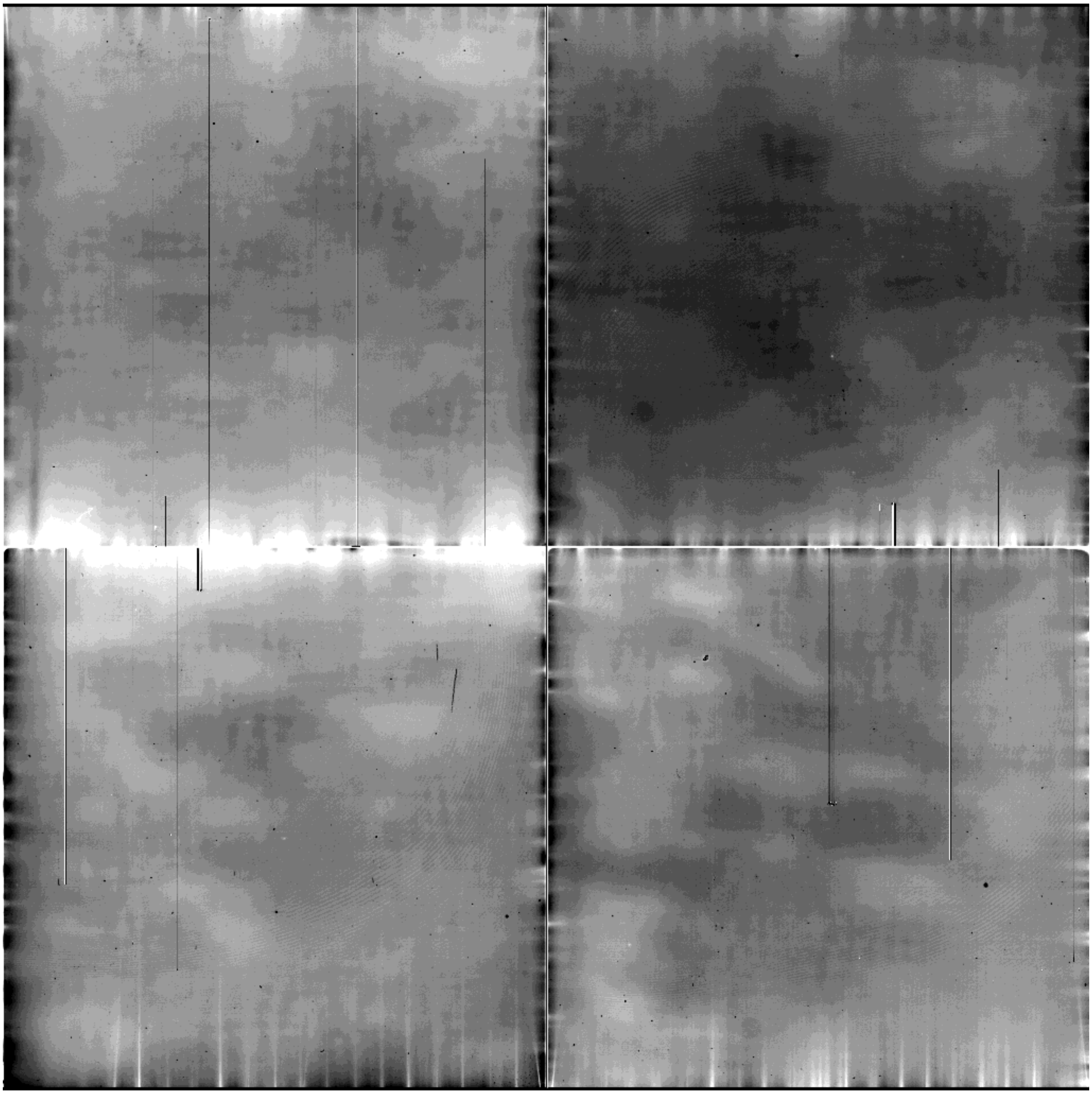

Figure 4: Flat field properties at 1060nm, at a level of 54Ke^{-}/pixel. The grey-scale cuts are set to $\pm 8\%$ of the median level.

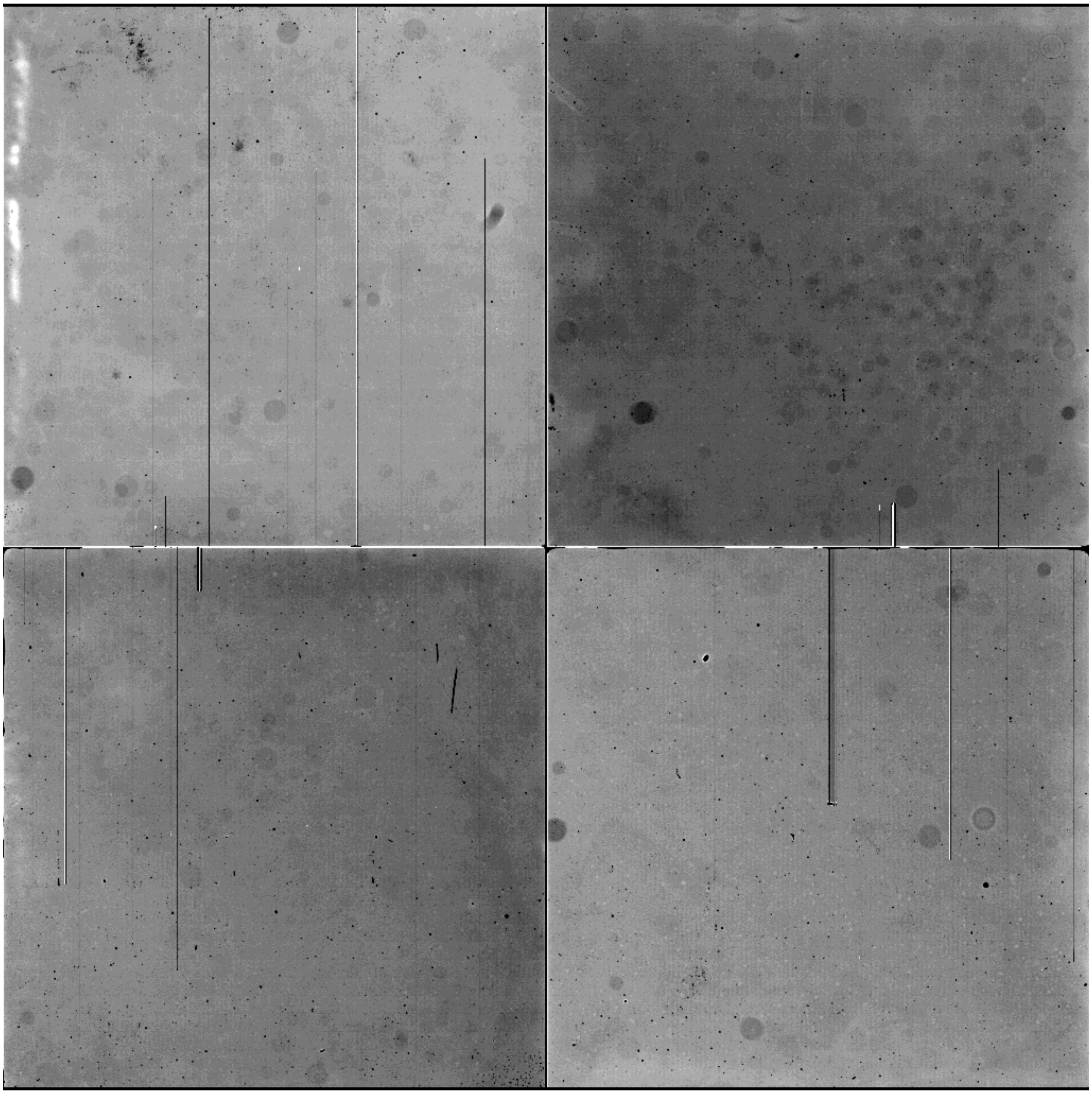

Figure 5: Flat field exposure for 550nm light, at a level of $65Ke^-$/pixel. The grey-scale cuts are set to $\pm4\%$ of the median level. It will be demonstrated later that the NW quadrant is partially saturated at this level.

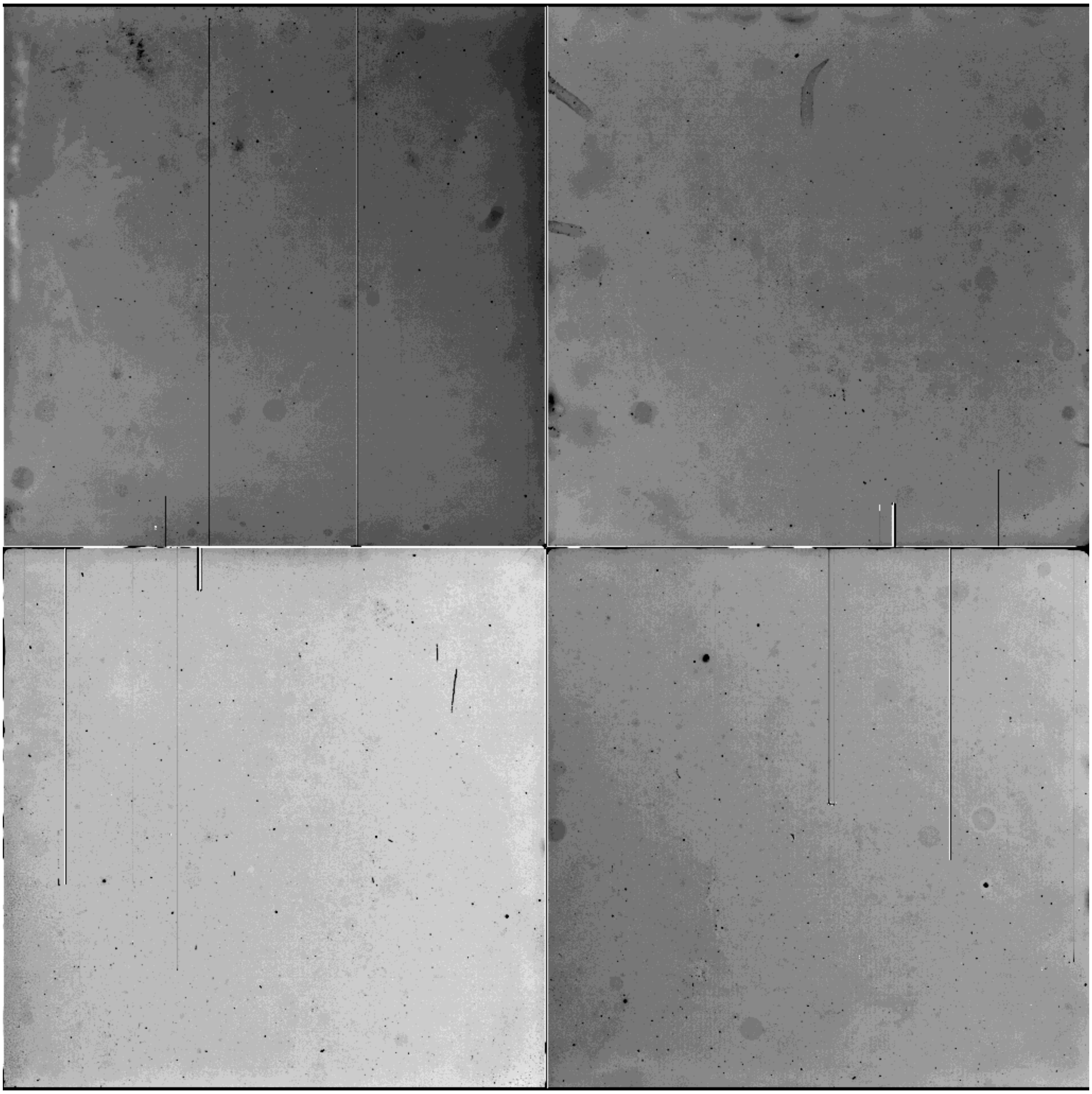

Figure 6: Flat field in 334nm illumination, at a level of $36\mathrm{Ke}^-$/pixel. The grey-scale cuts are set to $\pm 8\%$ of the median level.

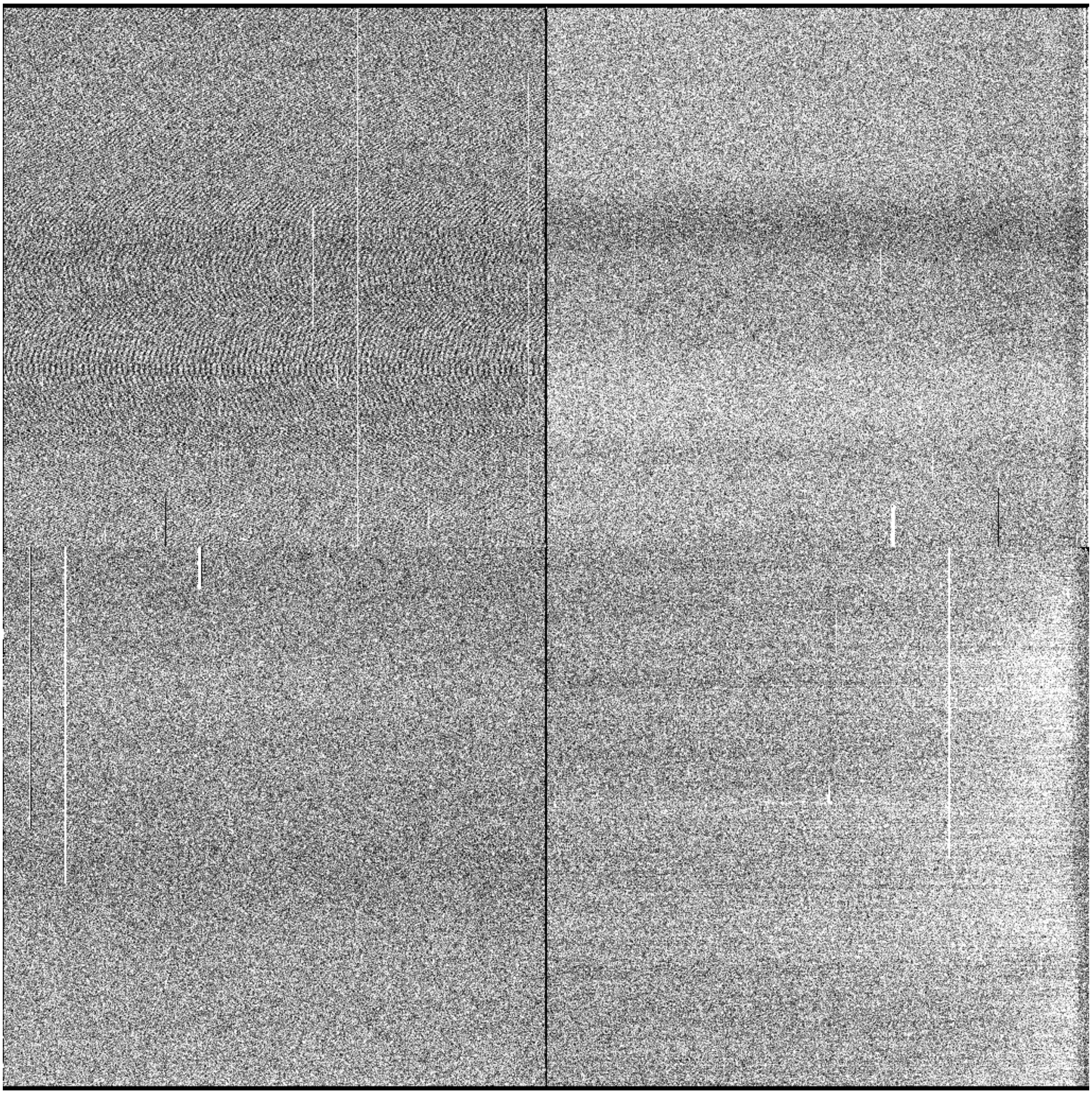

Figure 7: Ratio of 550nm high and low illumination flat fields, in order to identify charge traps. The high level flat field was median combined from 6 exposures with about 50Ke$^-$/pixel, and the low level was combined from 6 exposures with about 50e$^-$/pixel. The ratio is displayed with grey scale cuts of $\pm$ 10% of median level. Some variations due to bias level instability are visible in the eastern quadrants.

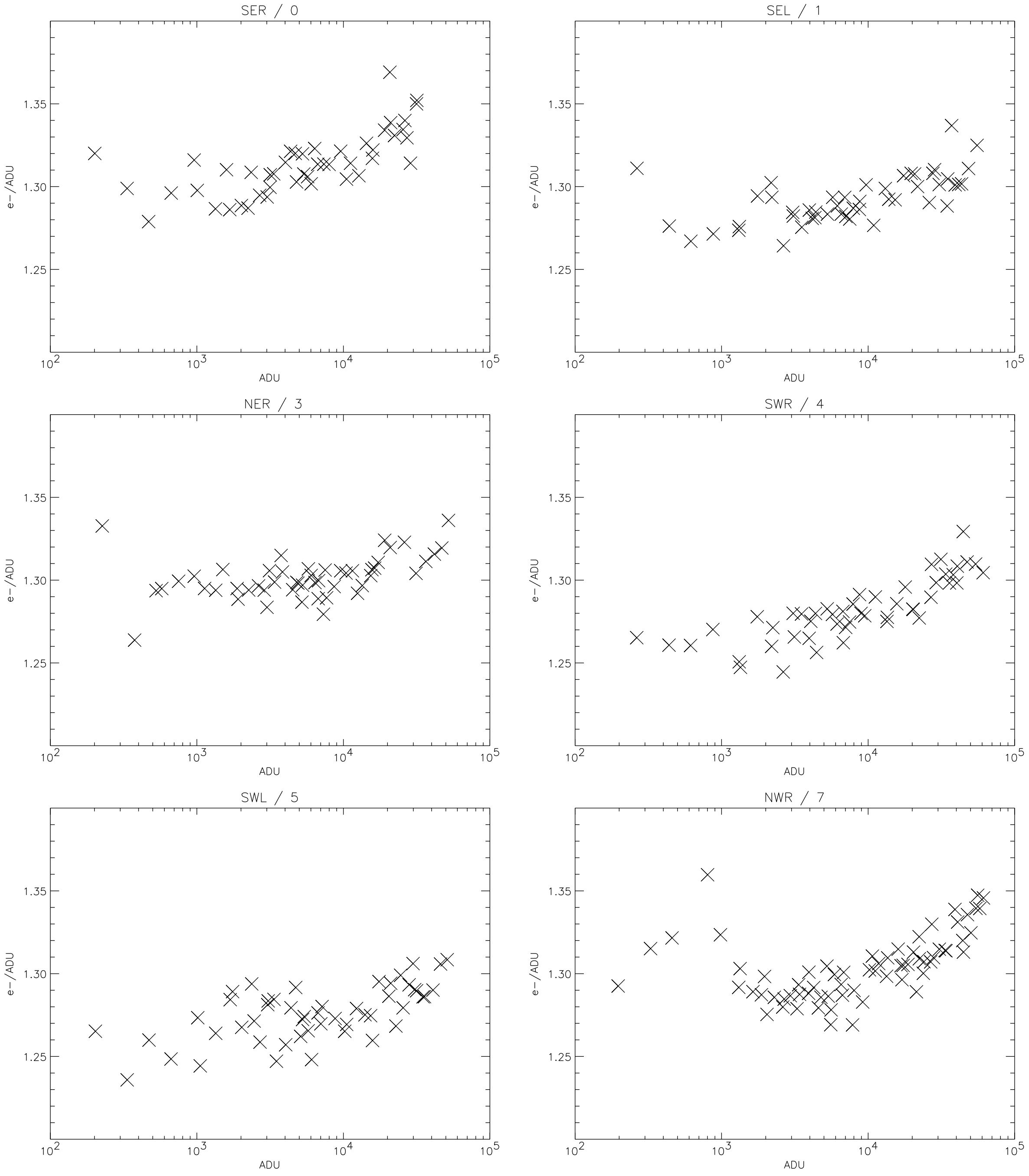

Figure 8: Gain versus exposure level measured from noise statistics for the six functional amplifiers in high-gain mode. The apparent slight increase of gain with exposure level is caused by an inadequate noise model. In fact, the gain is quite constant.

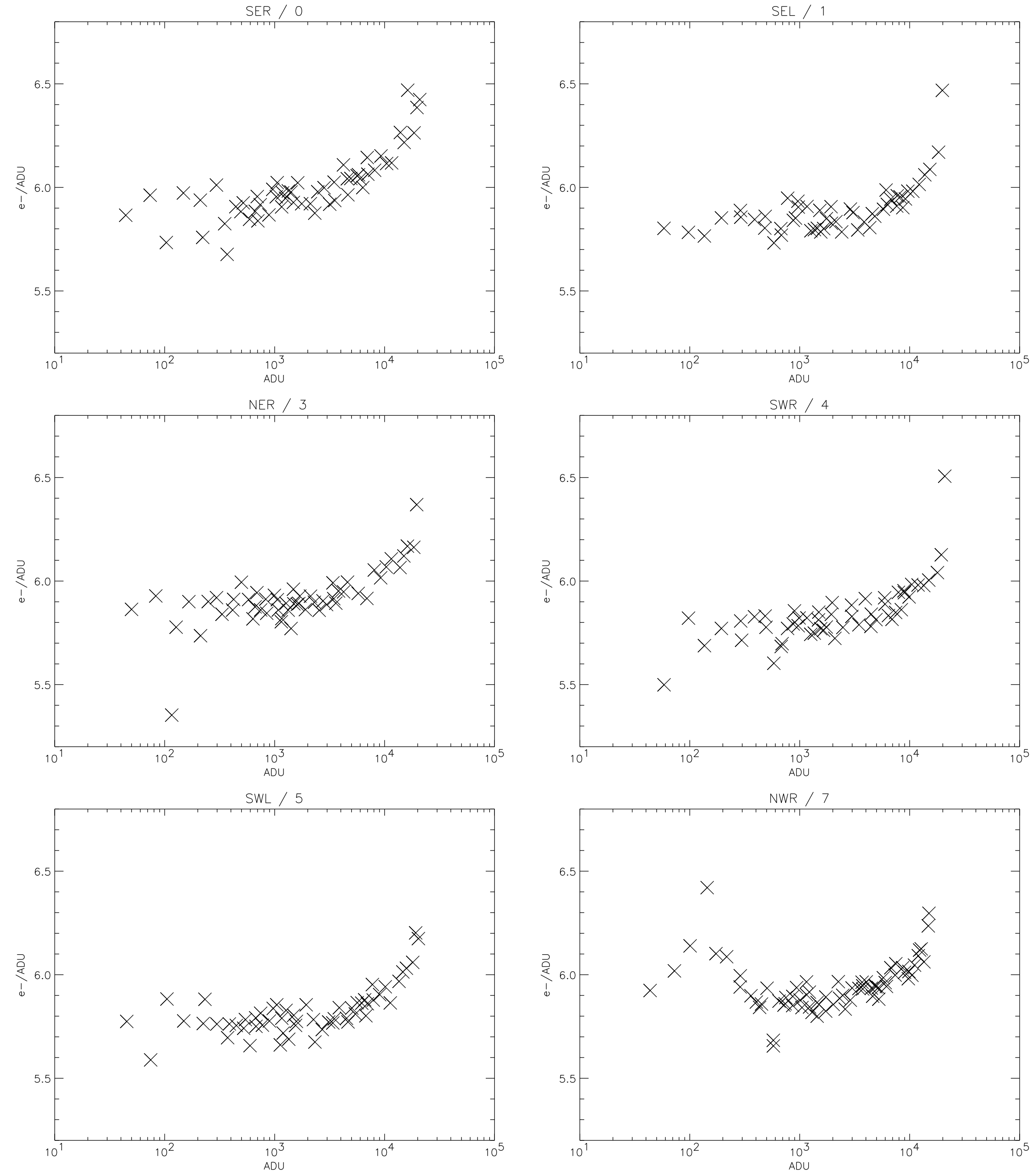

Figure 9: Gain versus exposure level measured from noise statistics for all six amplifiers in low-gain mode.

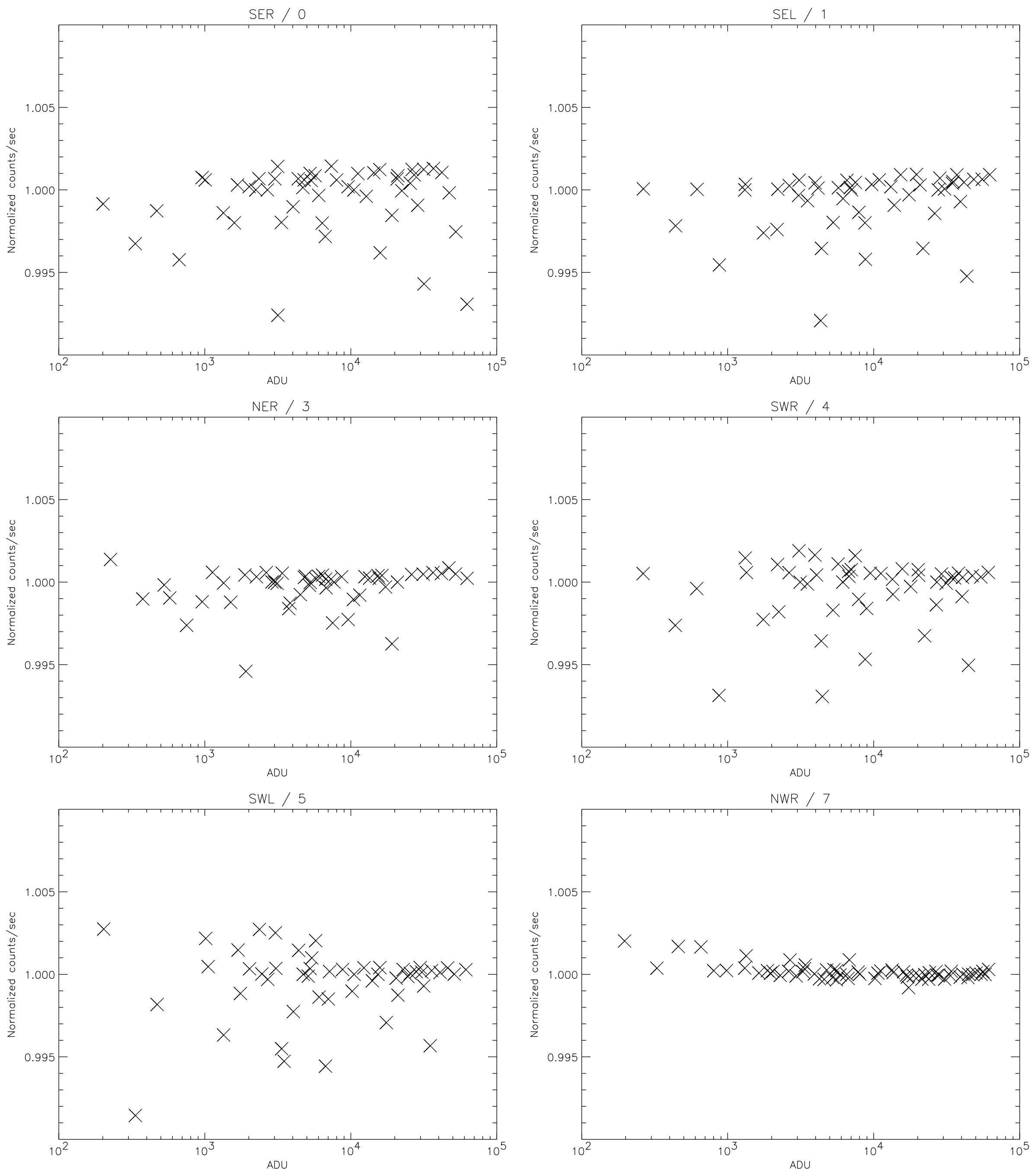

Figure 10: A plot of ADU per second versus total exposure time for each amplifier in high gain mode. The lower scatter for channel no. 7 is due to better stability of the linearity measurement, not better performance of the CCD output.

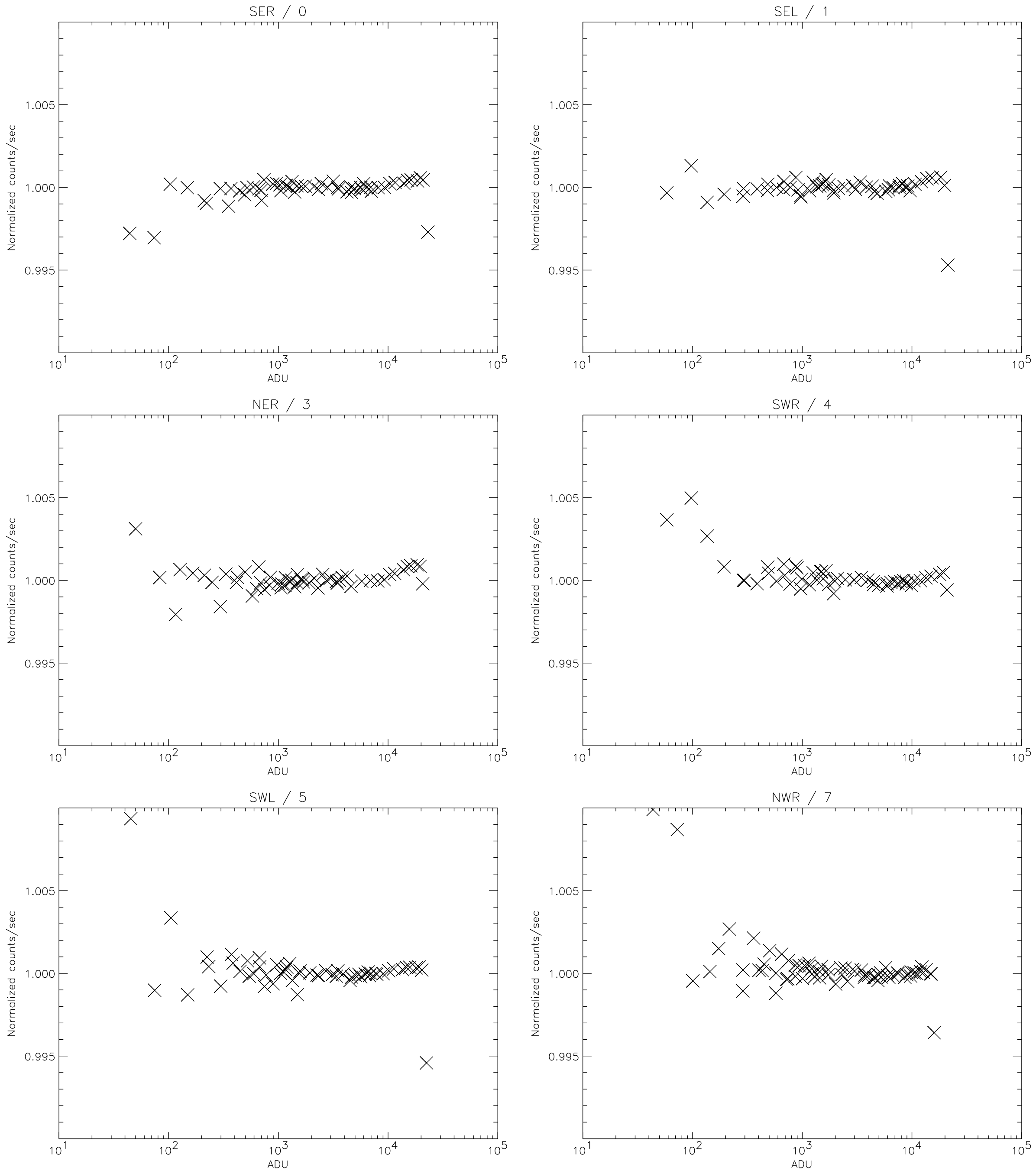

Figure 11: A plot of ADU per second versus total exposure time for each amplifier in low gain mode.

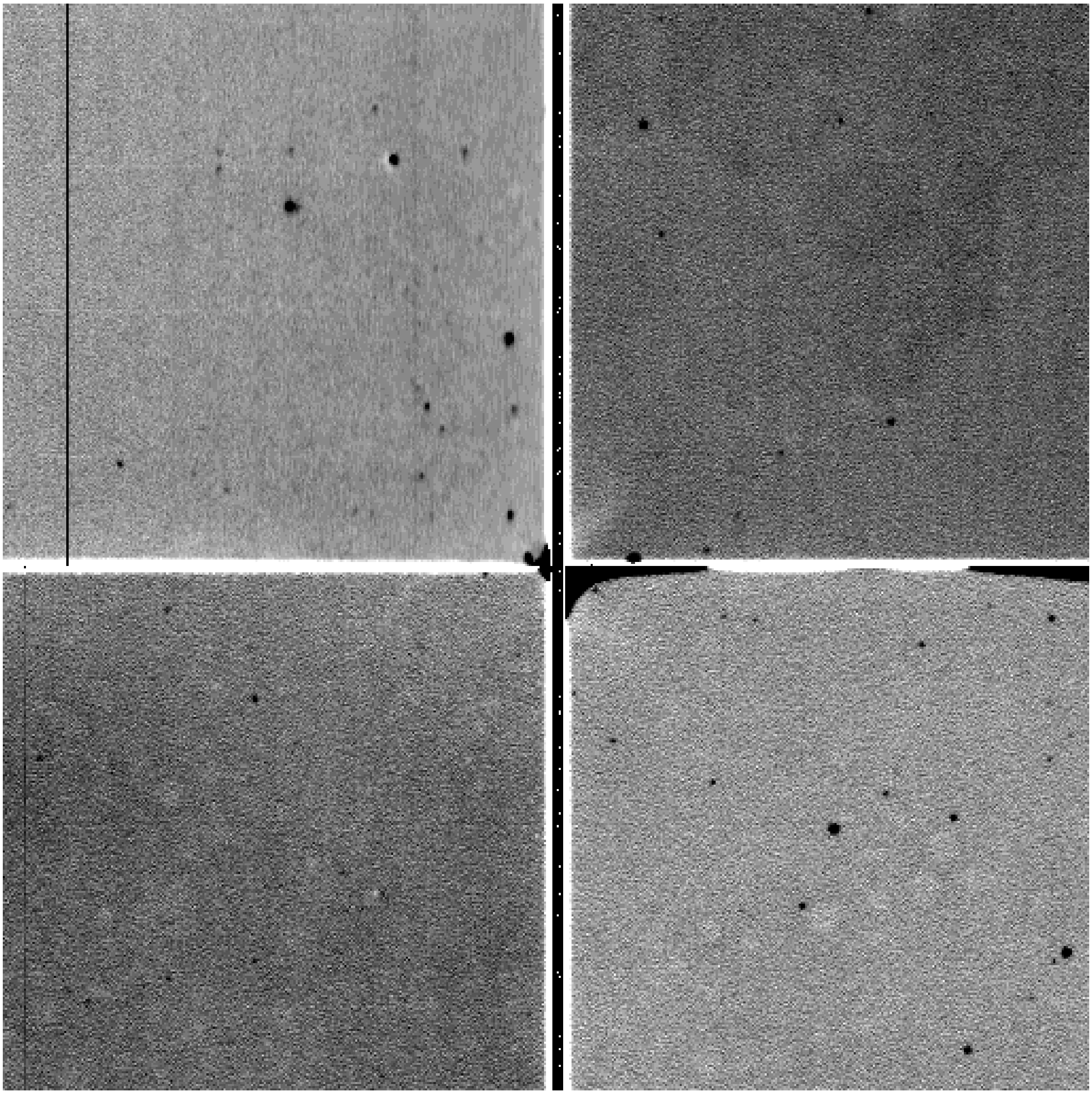

Figure 12: Central 512x512 pixels of a 550nm flat field, displayed with grey scale cuts of ± 4% of median level. The illumination level is about 50KADU or 65Ke$^-$/pixel. Note that the center-most corner of the NW quadrant appears smeared in the vertical direction, in contrast to the pixel-to-pixel variations in the surroundings. This marks the onset of blooming full well for the W20-(0,0) CCD.

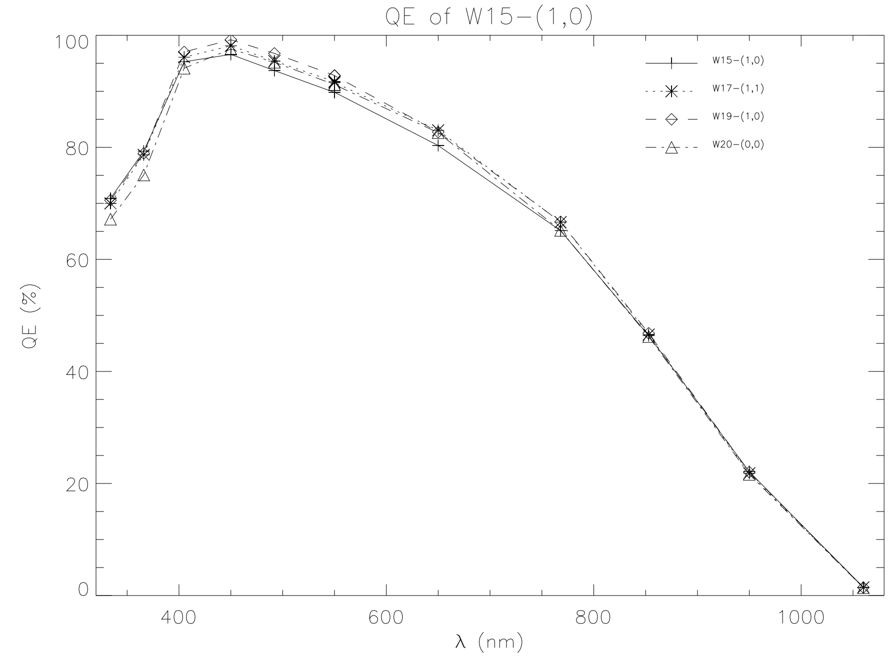

Figure 13: Global quantum efficiency versus wavelength for the four detectors. The distribution of sensitivity is quite similar for all devices.

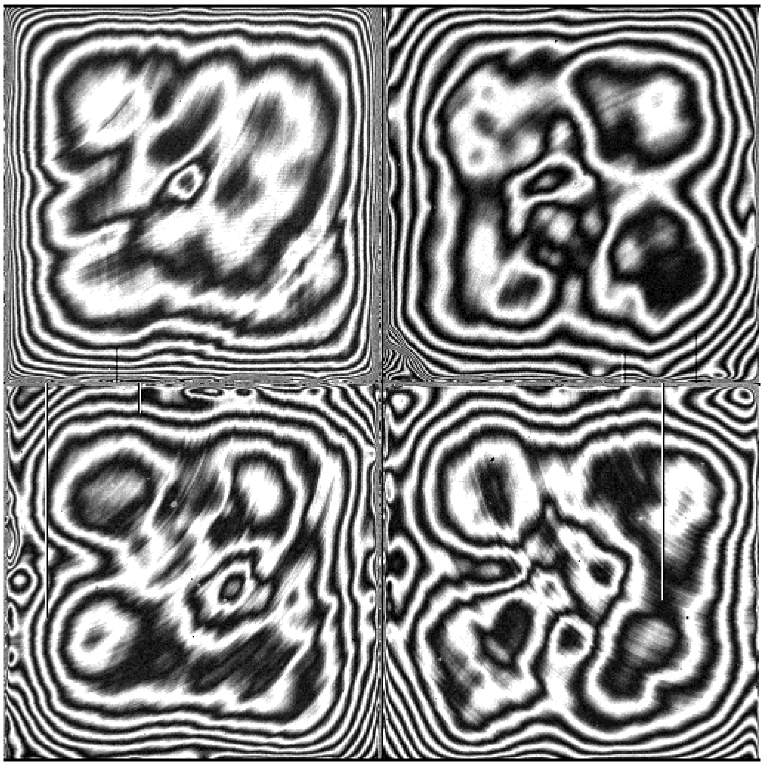

Figure 14: Fringing from 830nm monochromatic illumination. The grey-scale cuts are set to ±15% of the median level.

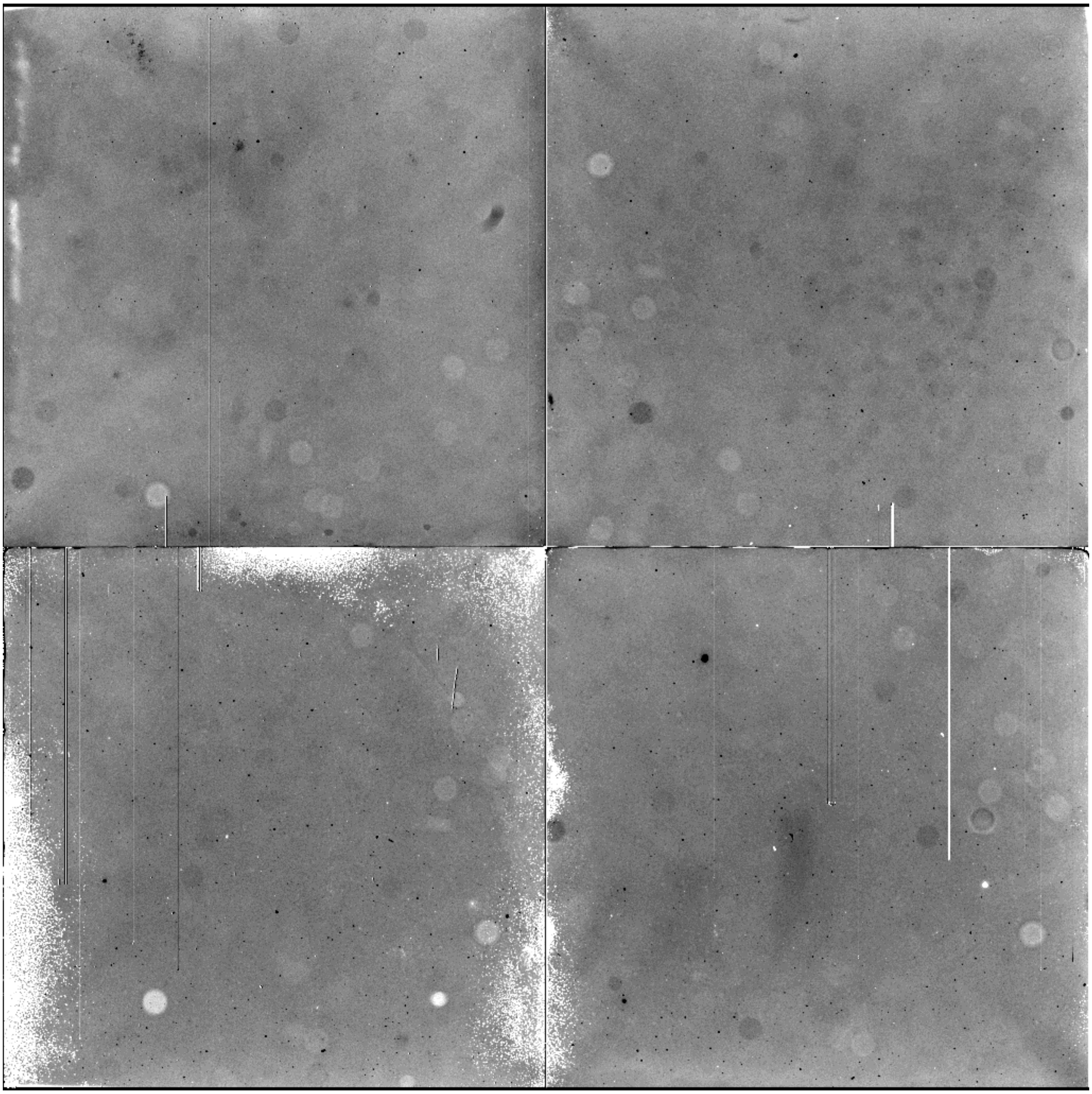

Figure 15: Ratio of 334nm flat fields from June/July 1998 and September 2002, i.e. a four year time-span. The ratio is displayed with grey scale cuts of ± 5% of median level. Bright areas are where the new flat field has higher sensitivity than the old one.

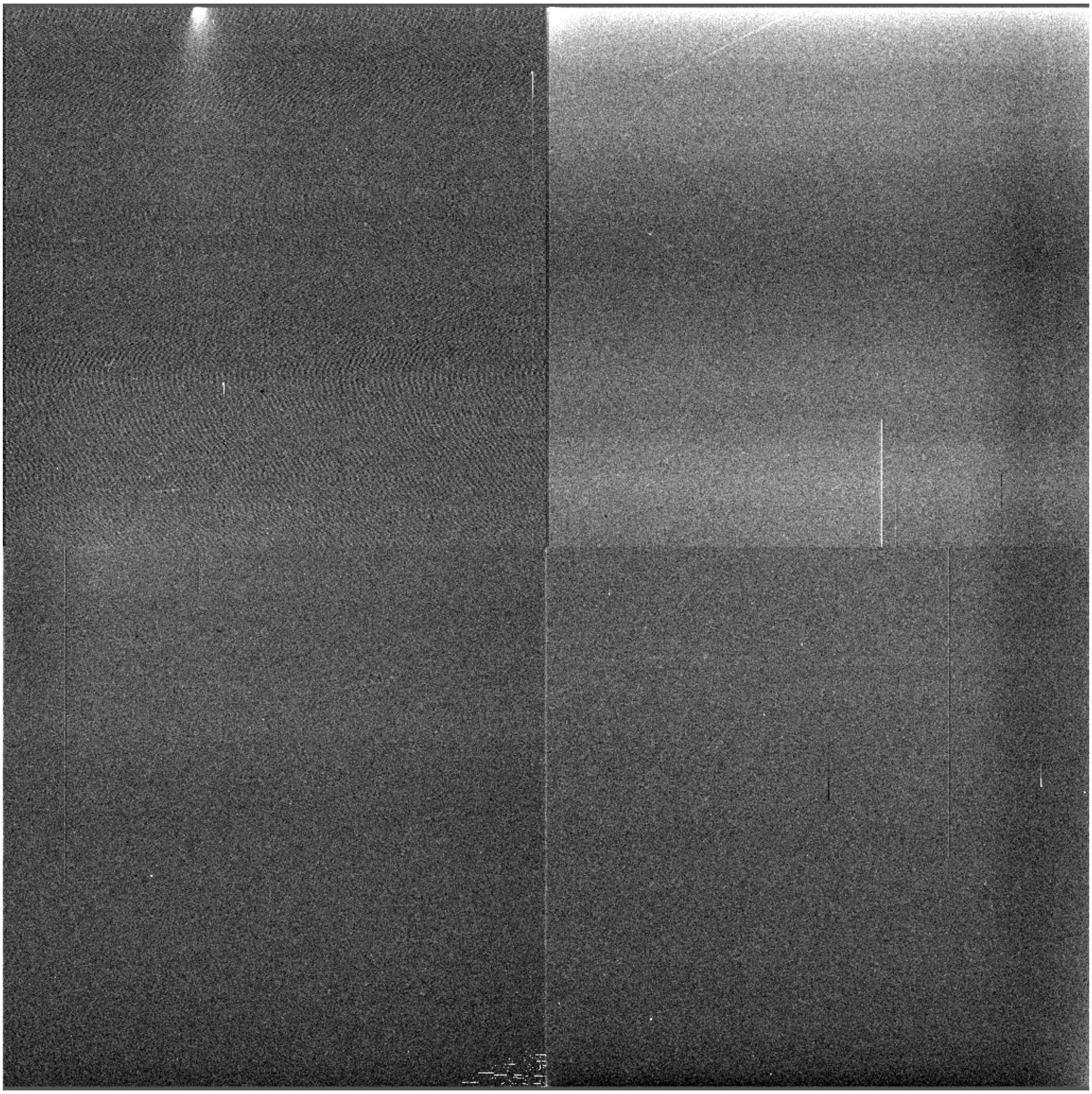

Figure 16: A median-combined image of six 30 minute dark exposures at a detector temperature of -100°C, MPP mode. The read-out configuration is A4RR. Grey-scale cuts are -5 to +10 ADU (approx. $-7e^{-}$ to $+13e^{-}$) relative to the bias level.

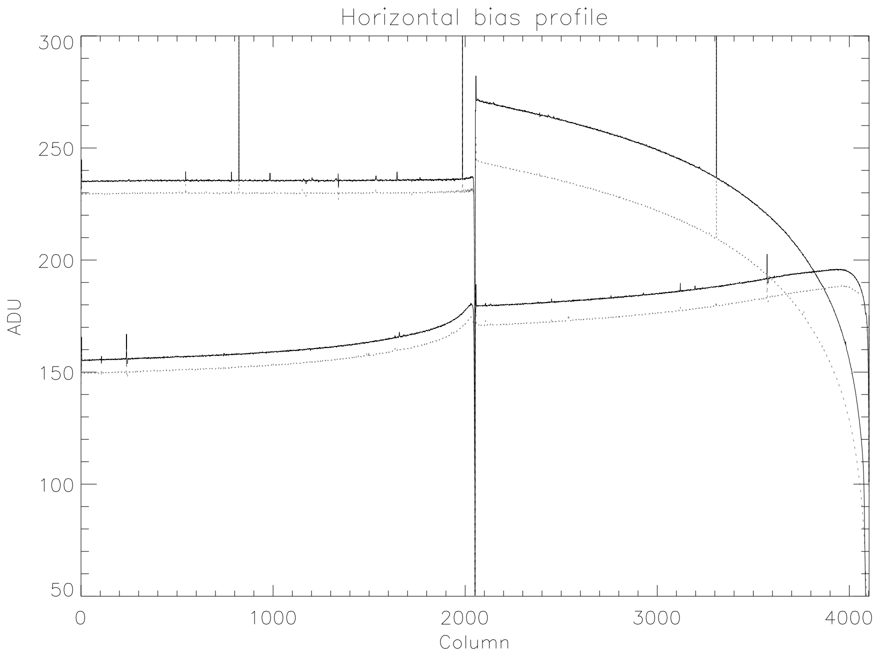

Figure 17: Horizontal profile of bias levels in the four quadrants, read out in A4RR mode. The northern quadrants are shown at a level of about 250ADU, and the southern are offset to 150ADU for easier reading. The full drawn line is a readout in the beginning of a sequence, and the dotted a readout about half an hour later.

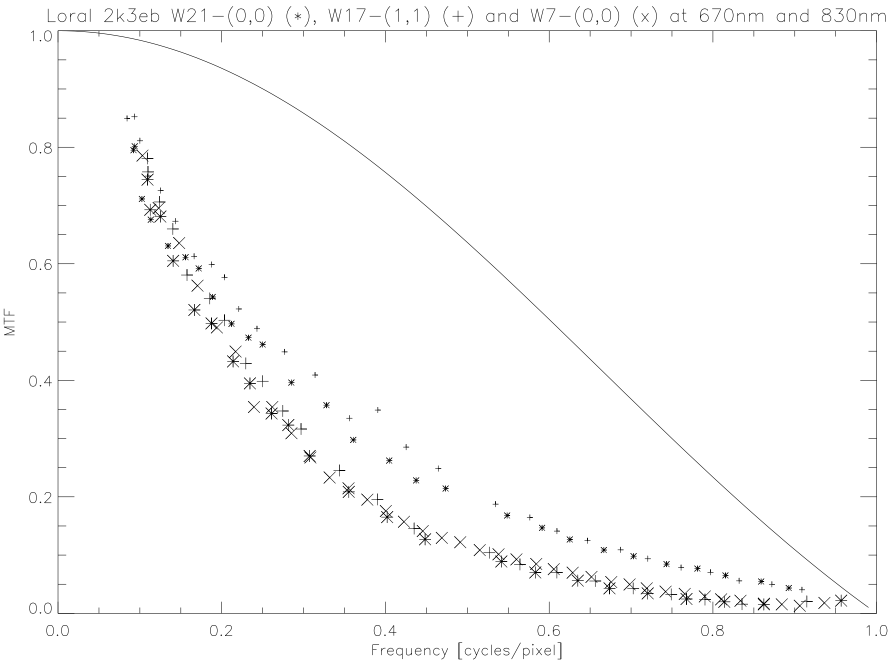

Figure 18: Modulation Transfer Function measurement for three representative CCDs at 670nm (large symbols) and 830nm (small symbols) illumination wavelength, compared to the ideal pixel response.